J. Mech. Phys. Solids, Vol. 46, No. 9, pp.1675–1697, 1998
©Elsevier Scinece Ltd. All rights reserved
Author prepared pre-print

APPLICATION OF DEBOND LENGTH MEASUREMENTS TO EXAMINE THE MECHANICS OF FIBER PUSHOUT

V.T. BECHEL and N.R. SOTTOS*

Theoretical and Applied Mechanics Department, University of Illinois at Urbana-Champaign, 216 Talbot Lab, 104 S. Wright St, Urbana 61801 U.S.A.

(Received 13 September 1996; in revised form 3 June 1997)

ABSTRACT

The interface failure sequence was observed during fiber pushout tests on several model composites. Composites with varying fiber-to-matrix moduli ratio (E_f/E_m), sample lengths, interface bond strength, and processing residual stresses were tested to determine which composites would debond from the top and which from the bottom. The present pushout experiments combined with previous work in the literature indicate that only composites with an E_f/E_m ratio greater than 4 tend to debond from the bottom during pushout testing, and debonding tends to initiate at the top of the interface when the E_f/E_m ratio is less than 3. The debond length as a function of force and displacement was also measured in a polariscope for two of the model composites—steel/epoxy and polyester/epoxy. The pushout data from a polyester/epoxy system that debonded from the top was fit to a shear lag solution of the fiber pushout problem to obtain the mode II toughness (G_{IIc}) of the fiber–matrix interface. The resulting interface toughness was then used to check the predicted debond length as a function of pushout force. The debond length calculated from the shear lag model was less than the measured debond length by a nearly constant 1.5 fiber radii.

Keywords: A. energy release rate, A. fracture toughness, B. fiber-reinforced composite material, B. friction, C. mechanical testing

1. INTRODUCTION

1.1. *Designing composites for damage tolerance*

The interface strength and friction coefficient, along with constituent elastic properties, volume fraction, and residual stresses, determine the performance of a continuous fiber-reinforced composite. Models developed to predict the uniaxial stress–strain curve (Daniel *et al.*, 1993) and the fracture toughness (Bao and Song, 1993) for a composite material require all of the above information. Daniel and co-workers showed that the uniaxial stress–strain curve for an SiC/calcium aluminosilicate composite loaded in tension parallel to the fibers has two large changes in slope due to matrix cracking and partial fiber debonding. Analytical models were proposed to correlate the failure mechanisms with the measured monotonic load–strain curve. Bao and Song showed that mode I fracture toughness for a composite is explicitly dependent

*To whom correspondence should be addressed. Fax: 217 244 5707

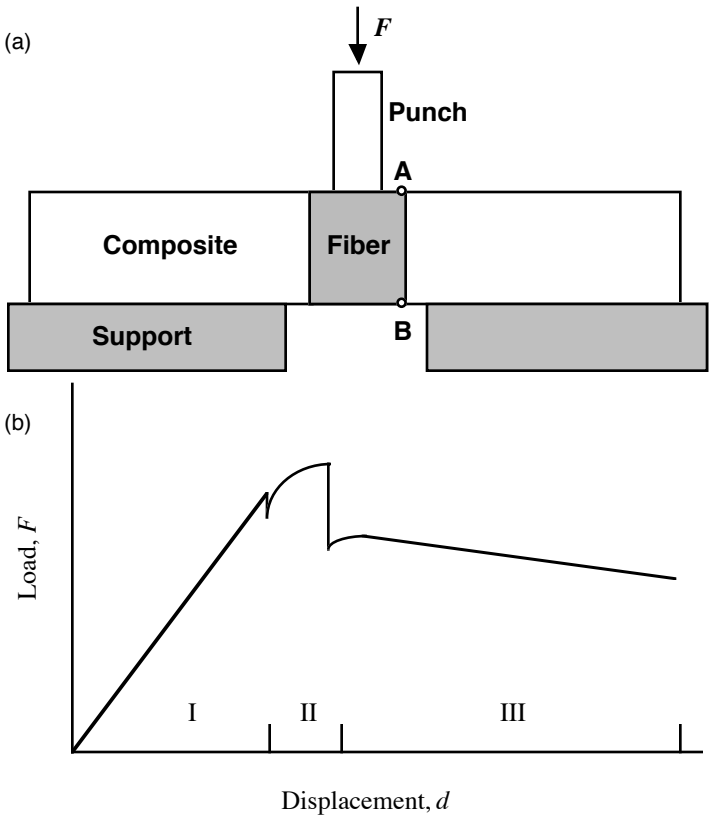

Fig. 1. The fiber pushout test: (a) schematic of the fiber pushout test, (b) schematic of a typical fiber pushout load–displacement curve.

on the size of the region of intact fibers (bridging zone length) ahead of a crack tip present in a composite under tensile loading parallel to the fibers. The bridging zone length was in turn shown to be dependent on not only the fiber strength but also the fiber–matrix interfaces capacity to transfer shear stress before and after debonding. The fiber and matrix elastic constants as well as the sample geometry are usually known for a composite, and the residual stresses away from the fiber ends can be calculated. Since the interface properties are not known for most fiber–matrix–coating combinations as a function of processing conditions, an experiment must be conducted to obtain the interface strength and friction characteristics. Ideally, a simple test would be conducted on a composite to find the fiber–matrix interfacial properties to be used as input for the models that are available to calculate composite toughness and extension under uniaxial tension. The composites response to loading could then be predicted for an arbitrary volume fraction.

One of the most popular tests to find interface properties is the fiber pushout test, which consists of pushing a single fiber out of a thin slice of composite material, while measuring applied force and pushout tool displacement (Laughner*et al.*, 1986; Netravali*et al.*, 1989; Brun and Singh, 1988; Warren*et al.*, 1992). Figure 1(a) shows a schematic of the pushout test. The popularity of the fiber pushout experiment is

derived from the ease of sample preparation, the wide range of composites to which the test can be applied, and the interface properties that can be computed from test data.

A composite is fabricated exactly as it would be for service, and a slice is sectioned for use as a pushout test specimen. Since multiple fibers may be present in a specimen, a particular fiber is chosen and aligned over a hole so the bottom surface of the fiber is traction free. The force–displacement curve recorded during the test is later related to interface mode II toughness and the coefficient of friction (assuming a Coulomb friction formulation) between the fiber and matrix by fitting it to one of the solutions to the fiber pushout problem available in the literature. The typical profile of the experimental curve from a pushout experiment is plotted schematically in Fig. 1(b). The force–displacement curve can be divided into three distinct sections. In section I it is thought that the interface is completely bonded, while in section II an interface crack is assumed to be growing. Finally, section III is believed to correspond to a completely debonded interface. In section III the fiber slides against the frictional force generated in the fiber–matrix interface.

Approximate solutions to the fiber pushout problem have been developed by Gao*et al.* (1988), Marshall and Oliver (1990), Liang and Hutchinson (1993), Kerans and Parthasarathy (1991), and Hsueh (1990). The solutions by Liang and Hutchinson and Kerans and Parthasarathy, subsequently referred to as the LH&KP solution, are identical for a composite with an isotropic fiber and matrix and represent the most advanced solution containing the shear lag assumption. No free surface effects, uniform residual stresses in the fiber and matrix with respect to axial position, and a critical compressive fiber axial stress as the criterion for debond are assumed. The LH&KP solution applies only to composites that initially debond from the top face of the sample (punch side). The debond must continue to grow along the interface toward the bottom without a bottom debond appearing at any point during the fiber pushout test.

1.2 *Complications inherent in the fiber pushout test*

The fiber pushout test is not free from difficulties. Koss*et al.* (1993) and Eldridge (1995) discovered that in selected metal matrix composites, the interface initially debonded from the bottom during the pushout test. The location of initial debonding was determined by interrupting the pushout test before the peak load and examining the top and bottom surface. The superposition of thermal residual stresses due to processing and mechanical pushout stresses produces a bottom debond for some combinations of fiber and matrix elastic properties, interface strength, and sample length.

As shown schematically in Fig. 2, the residual interfacial shear stress has the same sign at the bottom face of the sample as the interfacial shear stress produced by a pushout load and the opposite sign at the top of the sample. When the interfacial residual stress is large enough, the combined effect of processing a pushout load can lead to a bottom debond. The bottom debonding mechanism of Fig. 2 considers only interfacial shear stress, but other mechanisms such as tensile residual radial stress near the top and bottom of the fiber and tensile radial stress at the bottom of the interface due to sample bending could also contribute to a bottom debond. Although the experimental force–displacement curves from a pushout test on a system that initially debonds from the top and from one that initially debonds from the bottom

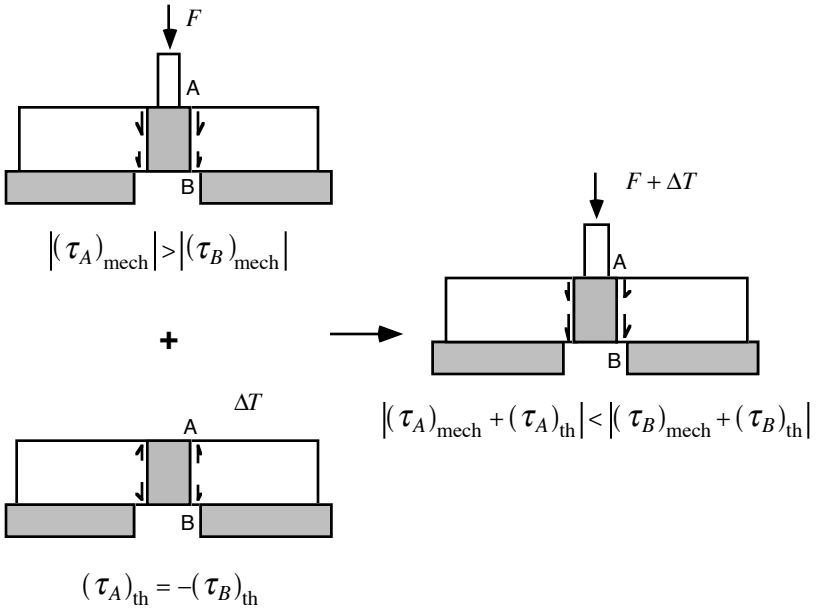

Fig. 2. Schematic of the interfacial shear stress near the top and bottom of a sample for a pushout load, a thermal load due to processing, and a combined pushout and thermal load.

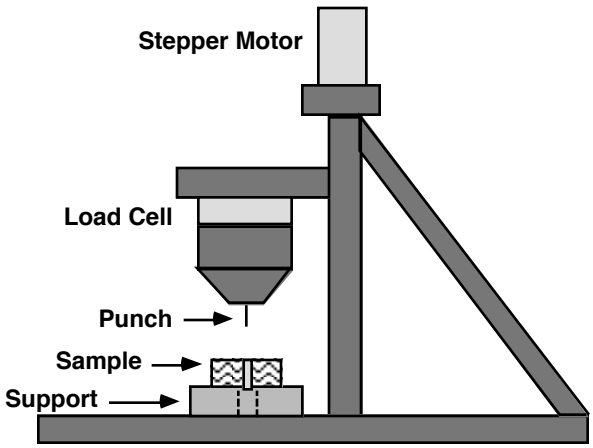

Fig. 3. Schematic of the micromechanical test apparatus used to perform pushout tests on model composites.

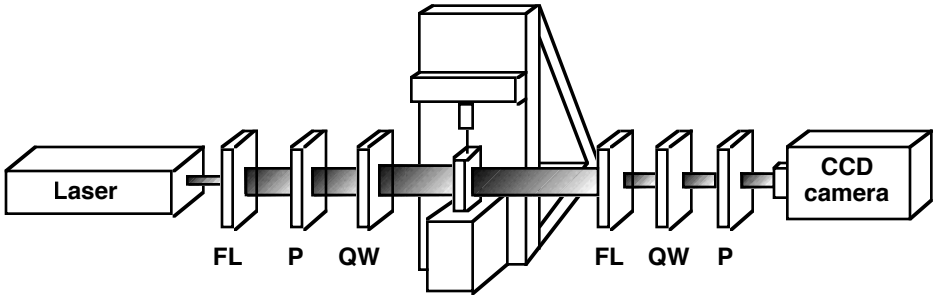

Fig. 4. Pushout apparatus positioned in the circular polariscope.

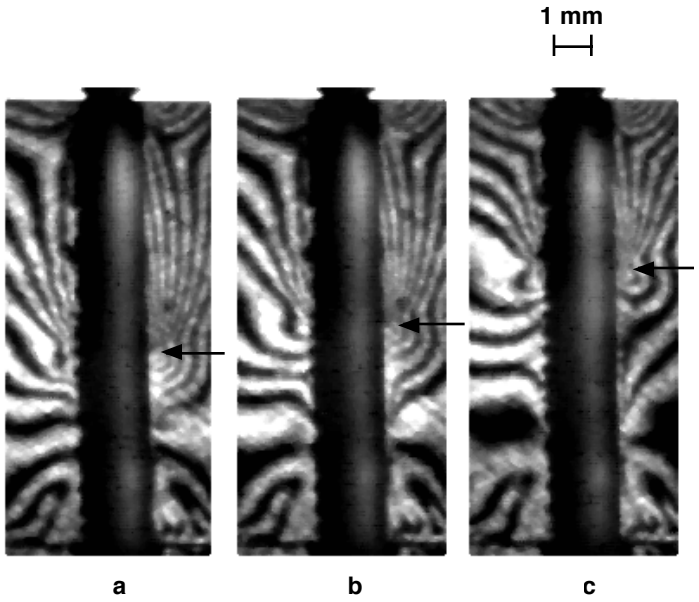

Fig. 5. Photoelastic images acquired during a steel/epoxy pushout test.

may have the same features (compare Figs. 6 and 8), the shear lag solutions available to date do not apply to the bottom debonding composite.

In addition to interface strength and friction coefficient, the roughness of the fiber surface, the differential shrinkage between the fiber and matrix due to cool down from processing temperature, and the chemical shrinkage of the matrix during processing may not be known accurately prior to the pushout test. These factors often significantly influence the force–displacement curve and are sometimes derived from the pushout experiment. Evidence that fiber surface roughness can increase the radial compressive stress on the fiber once the uneven fiber surface slides with respect to the matrix was found by Jero and Kerans (1990) when pushing fibers back to their original position in a composite. Also, Cordes and Daniel (1995) and Mackin*et al.* (1992) showed that interface wear during the frictional pushout portion of the pushout test can cause difficulties when modeling the coefficient of friction

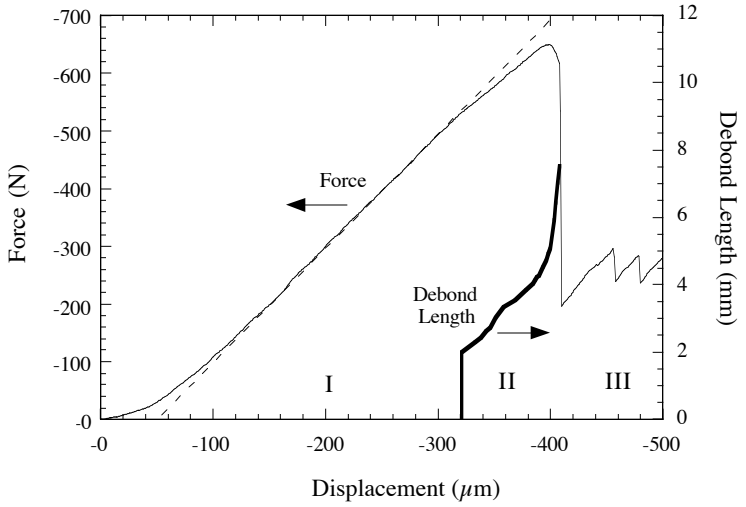

Fig. 6. Force and debond length versus displacement curves from a steel/epoxy pushout test. Debond was from the bottom. Fiber diameter = 1.65 mm, sample thickness = 13 mm, support hole diameter = 2.05 mm, and punch diameter = 1.4 mm.

and the radial stress from processing as constants. Even when a model is developed that includes all of the above variables, several variables may be fit to one curve. Fitting more than one property to one portion of the curve shown in Fig. 1(b)—although sometimes unavoidable—may produce inaccurate results from a theory that is formulated correctly.

In the pushout experiments reported in this paper, only the interface strength is fit to the progressive debonding portion of the pushout curve (section II), while the coefficient of friction is fit to the maximum load in the frictional part of the pushout curve so that the effects of wear are minimized. The matrix compressive radial stress away from the fiber ends due to processing is measured photoelastically before progressive debonding occurs and after total debond so that the additional radial stress at the interface due to fiber surface roughness is accounted for (found to be negligible for polyester/epoxy).

Several previous investigations have been carried out with the intention of gaining a clearer understanding of the fiber pushout experiment and how to analyze the resulting data. Some of this research employed the fiber pullout experiment in which a single fiber is pulled from a composite rather than pushed out. The mechanics of the fiber pullout experiment are similar to fiber pushout, and pullout experimental curves have the same general profile as the schematic of a pushout curve shown in Fig. 1(b) so relevant fiber pullout research has been included in the literature review. Tsai and Kim (1991, 1996) used a polariscope to study the stick–slip phenomenon in the frictional part of the pullout test (section III) for an optical glass fiber in an epoxy matrix. Watson and Clyne (1992) investigated the stresses produced during pushout testing before debond (section I) in an epoxy/epoxy model composite also

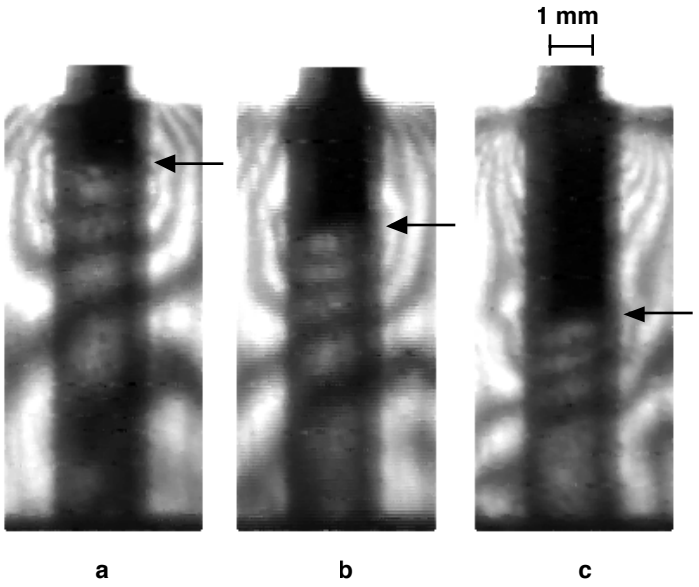

Fig. 7. Photoelastic images acquired during a polyester/epoxy pushout test.

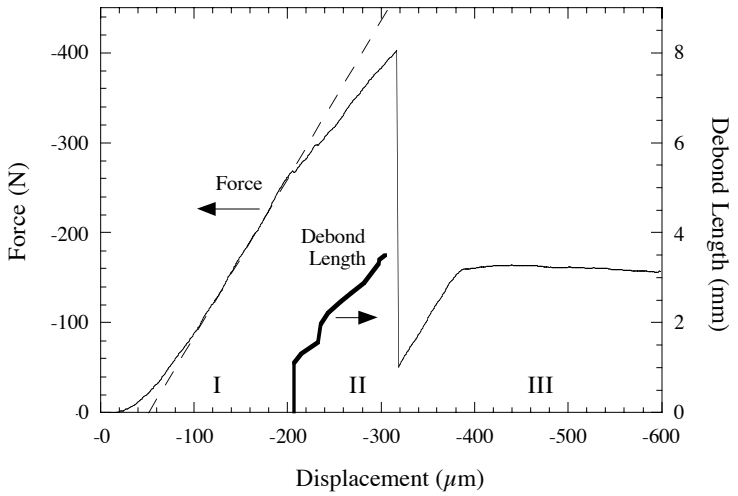

Fig. 8. Force and debond length versus displacement curves from a polyester/epoxy pushout test. Debond was from the top. Fiber diameter = 1.9 mm, sample thickness = 5.3 mm support hole diameter = 2.05 mm, and punch diameter = 1.7 mm.

using a polariscope. Atkinson*et al.* (1982) pulled a glass rod from a polyurethane matrix. By tracking photoelastic fringes, debond length was determined throughout the pullout test, but stable debond growth from the top was never achieved. Several debond lengths were input in a finite element model and a force–displacement curve with the same trends as the experimental curve (somewhat stiffer) was analytically produced. The converse procedure of predicting debond length from the experimental results was not attempted. Finally, Cordes and Daniel (1995) measured the debond length as a function of force in a fiber pullout test for an SiC fiber in a glass matrix by observing a change in the intensity of light reflected from the fiber surface when the interface debonded. The data were fit to the LH&KP solution. Because interface wear was significant, a negative coefficient of friction was predicted by the shear lag solution.

In the current study, the interface failure sequence is observed during fiber pushout tests on model composites. Model composites consisting of various fibers in a birefringent epoxy matrix were chosen because the interface failure sequence and the debond length are determined by inspection of photoelastic fringe patterns in the matrix. This observation allows the correspondence between the characteristics of the force–displacement curve and the interface failure processes to be identified. The applicability of the LH&KP shear lag solution is determined by noting the initial debond location and comparing measured to predicted debond length.

2. FABRICATION OF MODEL COMPOSITES

Several types of model composites were fabricated for the pushout experiments. Many combinations of materials, sample lengths, and support hole diameters were pushout tested to determine the most important parameters in producing a top or bottom debond. Single fiber samples of tool steel, borosilicate glass, quartz, nylon, glass particle reinforced nylon, and polyester fibers in an epoxy matrix were fabricated. An epoxy matrix was chosen for the photoelastic observations because of its high material fringe constant and ease of sample preparation. As shown in Table 1, these constituents correspond to a composite range of 0.81–0.83. Three different curing agents—diethylenetriamine (DETA), p-aminocyclohexylamine (PACM), and bis-1-propanamine (Ancamin 1922) were used to cure EPON 828 epoxy resin and vary the differential shrinkage strain during processing from 0.0022–0.0084. The DETA/EPON 828 and Ancamin 1922/EPON 828 systems were cured for 7 days at room temperature, and the PACM/EPON 828 system was cured for 2 h—the first hour at 80°C and the second hour at 150°C. To vary the interface strength some fibers were uncoated, some were coated with a silane to increase the interface strength, and some were coated with a silicone release agent to produce a very weak interface.

Samples were prepared by positioning a single fiber lengthwise in an 8 mm wide $\times$ 25 mm long mold and pouring a mixture of resin and curing agent into the mold. After curing, the front and rear faces of the sample were polished to a 15 μm finish. The pushout samples were then cut from the bulk sample to lengths ranging from 2.5–25 fiber diameters. The range of lengths for each composite depended on the particular fiber used, e.g., the 1 mm diameter glass fiber allowed the glass/epoxy samples to be cut to a maximum length of 25 fiber diameters. The fiber diameters are listed in Table 1.

Table 1. Model composite fiber-to-matrix moduli ratios and processing induced residual strains

Fig. 9 label	Model fiber (diameter in mm)	Epoxy matrix	E_f/E_m	Processing ΔT (°C)	Residual strain ($\Delta\epsilon_r$)
1	Polyester (1.95)	EPON 828 + DETA	0.81	0	-0.0022*
2	Nylon (1.5)	EPON 828 + DETA	1.70	0	-0.0022*
3	Glass reinf. nylon	EPON 828 + Anc.1922	3.06	0	-0.0030*
4	Glass reinf. nylon (1.5)	EPON 828 + PACM	3.31	-125	-0.0056**
5	Borosilicate glass	EPON 828 + DETA	16.3	0	-0.0022*
6	Borosilicate glass (1.0)	EPON 828 + PACM	22.0	-125	-0.0081**
7	Quartz (1.0)	EPON 828 + PACM	29.0	-125	-0.0084**
8	Steel	EPON 828 + DETA	50.0	0	-0.0022*
9	Steel (1.65)	EPON 828 + PACM	83.0	-125	-0.0072**

*Matrix chemical shrinkage.
**Processing $\Delta\alpha\Delta T$.

Finally, the samples were placed on a steel support such that the fiber was centered over a hole. The support hole diameter was less than 1.25 fiber diameters for all the pushout tests including the tests on the nylon, glass, and quartz/epoxy systems for which the location of initial debond was determined, but the debond length was not measured. Force and debond length as a function of displacement were measured for polyester/epoxy and steel/epoxy only, and the exact support hole diameter (along with the other relevant dimensions) is provided with the force–displacement–debond length results for each of these composites.

3. EXPERIMENTAL APPARATUS

A micromechanical tester was designed for performing the pushout experiments in a polariscope. Figure 3 shows a schematic of the pushout apparatus. The tester consists of a Compumotor SX stepper motor and Daedal MS23 railtable. Displacement at the approximately 0.9 fiber diameter steel punch tip was measured by recording the commanded rotation of the stepper motor armature as a function of time and then carefully subtracting machine compliance. The punch velocity was maintained at 5 μm/sec. Load was measured by sampling a Kistler piezoelectric charge transducer at 5 samples/sec. The load cell signal was conditioned by a Kistler dual mode amplifier and digitized by a Tektonix TDS 420 oscilloscope.

The testing apparatus was positioned such that the pushout sample was entirely illuminated by a circular polariscope as shown in Fig. 4. The polariscope was constructed using an argon laser (Lexel model 3500) as the light source. Since coherent light can create interference fringes, a spinning ground-glass disk was used as a coherency scrambler. A collimated beam of light passed through a polarizer (P) which vertically polarized the light, and then through a quarter-wave plate (QW) with its fast axis at 45 degrees to the axis of the polarizer, producing circularly polarized light. The beam continued on through the specimen, traversed a second quarter wave plate 90 degrees out of phase with the first and through a second polarizer, eliminating the isoclinic fringes from the resulting image. Field lenses (FL) were inserted into the beam before and after the sample. The first field lens expanded the diameter of the beam from 2.5 mm to 25 mm, permitting a larger field of view, and the second field

lens focused the beam on the aperture of a CCD camera (Panasonic BL200). A 640 pixel by 480 pixel frame grabber was used to store the images at a maximum rate of 5 frames per second during the pushout test.

4. MEASUREMENT OF DEBOND LENGTH

After the pushout test was completed, the individual images were inspected to determine the debond length as a function of time so that the debond length could be plotted as a function of force and displacement. Debond length was measured for only one bottom debonding and one top debonding model composite of Table 1—steel/epoxy and polyester/epoxy, respectively. Figure 5 shows a representative series of images taken during a pushout test of a steel fiber in an epoxy (EPON 828 + PACM) matrix. The load increases from frame a–b–c. The black rod in the center of each frame is the model fiber. The gray areas to the left and right of the fiber containing the photoelastic fringes are a portion of the matrix near the fiber. A small section of the punch can be seen near the top of the fiber, and for clarity, this particular sample was mounted on an epoxy support so that the support hole could be observed at the bottom of the frames. The tip of the interface debond is the location along the interface of the greatest fringe density and is marked with an arrow in each frame. The debond can clearly be seen to grow from the bottom face of the sample toward the top face with increasing load.

Figure 6 shows the corresponding force–displacement curve for the steel/epoxy model composite. This system debonded from the bottom, and therefore could not be fit to the LH&KP shear lag solution to determine interface toughness. The steel/epoxy pushout curve contains a significant region of unstable debond growth between the peak load and total debond that is not found in the pushout curve from a top debonding composite (Fig. 8). The large stress gradients near the top surface apparently start interacting with the stress field around the crack tip within approximately 4 fiber diameters of the top surface. Figure 6 and the following pushout curve for polyester/epoxy (Fig. 8) both include a displacement from a machine compliance of 0.42 μm/N.

A representative series of images is shown in Fig. 7 for a polyester fiber in an epoxy (EPON 828 + DETA) matrix. Again, the load increases from frame a–c. For this system, the debond progressed from the top face to the bottom. Only one small fringe tracked the interface crack tip because the matrix residual stresses were much smaller than in the steel/epoxy system. The polyester/epoxy system offered an additional measure of debond length. Before debond the fiber was transparent, but once the fiber–matrix interface debonded, very little light passed through the debonded portion of the fiber. The photoelastic fringes and the darkened portion of the fiber indicated the same debond length. The corresponding load–displacement curve along with the measured debond length is shown in Fig. 8. The polyester/epoxy results are used in Section 6 to compare measured debond length with the debond length predicted by the LH&KP solution.

5. TOP VS BOTTOM DEBOND

In order to gain information about which composite systems will debond from the top and which from the bottom, model composites with varying E_f/E_m, sample

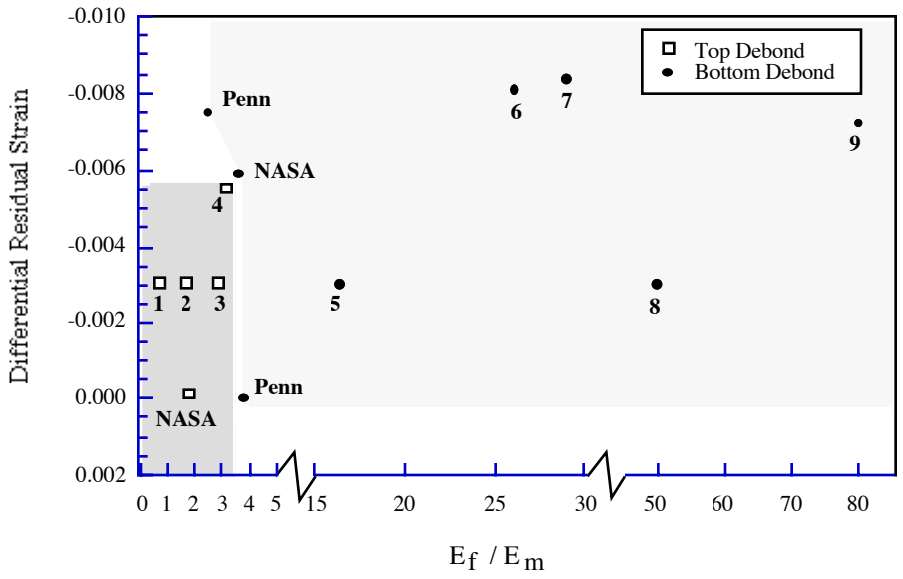

Fig. 9. Map of top and bottom fiber debonds as a function of fiber-to-matrix stiffness ratio and residual thermal strain.

length, interface bond strength, and processing induced residual stresses were tested (see Table 1 for constituent properties). Figure 9 shows a plot of initial debond location as a function of differential residual thermal strain and E_f/E_m ratio. The upper right shaded area contains the composite systems that initially debonded from the bottom during pushout testing, and the lower left shaded area represents the top debonding composites. Results from this work and from other pushout data in the literature are plotted. The numbered data points, as designated in Table 1, are from the current pushout experiments on model composites. The points labeled Penn correspond to tests done by Koss*et al.* (1993) on alumina/niobium and sapphire/TiAl composites, and the NASA points correspond to tests done by Eldridge (1995) on SiC fibers in a titanium alloy matrix and in a reaction bonded silicon nitride matrix.

The steel/epoxy, quartz/epoxy, and glass/epoxy samples all initially debonded from the bottom, and the debond grew from the bottom toward the top until total debond. A top debond did not appear at any point during the tests. Decreasing the interface strength with a silicone fiber coating, or decreasing the residual stresses with a room temperature cure epoxy did not produce a top debond. For a range of sample lengths of 2.5–25 fiber diameters for the glass and quartz fiber composites and 2.5–15 fiber diameters for the steel fiber composites a top debond was not produced. The increasing lengths and corresponding greater load required to debond the fiber eventually caused the fiber end to be damaged by the punch load (punch diameter approximately 0.9 fiber diameters).

In the polyester/epoxy, nylon/epoxy and glass reinforced nylon/epoxy samples a debond initiated from the top and then grew toward the bottom until total debond. Samples as short as 2.5 fiber diameters were tested without a bottom debond occurring. As with the bottom debonding systems, some fibers were coated with a silicone release agent and some with a silane to vary the interface strength, and the three

curing agent–epoxy resin combinations described in Section 2 were used to vary the residual stresses. A top debond was observed in all cases.

Most fiber pushout tests are not conducted on systems with transparent and/or birefringent matrices, so the plot in Fig. 9 may be useful when estimating whether the system being tested will debond from the top or bottom. Caution must be used when employing Fig. 9 to predict the pattern of debonding for a particular composite. The location of initial debonding depends on the sample support hole diameter, the interface strength, the details of the residual stress field, and the sample length in addition to the two parameters shown in Fig. 9 (E_f/E_m and $\Delta\alpha\Delta T$). All possible combinations of these parameters for the model composites could not be tested. Also, the NASA and Penn data points represent results for only a small range of sample lengths (2–4 fiber diameters), one sample support hole diameter, and one interface strength.

However, the information in Fig. 9 shows some interesting trends. A large E_f/E_m ratio increases the chance that the composite will debond from the bottom during pushout testing. Many composites of current interest will not debond from the top since a very low E_f/E_m ratio is required along with relatively low differential shrinkage during processing. For low differential residual thermal strain, as E_f/E_m increases, there is a transition from a top debond to a bottom debond that occurs within a range of E_f/E_m ratio from 3–4. As the residual thermal strain due to processing increases within the $3 < E_f/E_m < 4$ interval, the location of initial debonding again changes from top to bottom. The tendency shown in Fig. 9 for a bottom debond to occur under more severe processing conditions is in agreement with the bottom debonding mechanism described in Section 1.2 and illustrated in Fig. 2.

6. COMPARISON WITH A SHEAR LAG SOLUTION

The LH&KP shear lag solution was derived based on a debond from the top. Consequently, the measured debond length data from one of the model polyester/epoxy composites was chosen to compare with the shear lag predictions of debond length. The data used was from tests on the polyester/epoxy system with no fiber coating and a room temperature cure epoxy (DETA curing agent) because this system produced the largest range of stable debonding before loads were reached which caused permanent deformation of the top surface of the fiber. The pushout curve in Fig. 8 was used for the following comparison.

6.1 *Shear lag theory*

The shear lag assumption is the hypothesis that the change in axial stress in the fiber of a composite is due solely to shear stress transferred through the interface from the matrixhence the name "shear lag". Equilibrium of a fiber element in the axial direction is formulated as

$$dP(z) = -\tau_{rz}(r_f, z)(2\pi r_f)dz, \tag{1}$$

where $dP(z)$ is the axial load on the cross-section of the fiber at the axial position. The radial coordinate is r, and r_f is the radius of the fiber. In the LH&KP shear lag solution to the pushout problem, the interfacial shear stress, τ_{rz}, is formulated as the

sum of a term due to processing and a term due to Poissons expansion of the fiber under the compressive punch load. The following equation shows this relationship:

$$\tau_{rz}(r_f, z) = \mu \left[\sigma_N - k \frac{P(z)}{\pi r_f^2} \right]. \tag{2}$$

The coefficient of friction is μ, and the constant,k, is a combination of the elastic properties of the fiber and matrix and is given by Kerans *et al.* The thermal residual radial stress at the interface away from the ends, σ_N, is often calculated assuming plane strain, but in the current work, σ_N was measured as described in Section 6.2. The assumption of a constant σ_N would be most accurate for infinitely long samples, and for debond lengths that extend far from the top surface. Equation (1) and (2) are combined, and the resulting ODE is solved subject to $P(z) = F$ (where F is the force applied by the punch) at the top of the fiber to arrive at an equation which relates the debond length to the applied load:

$$l_d = \frac{r_f}{2\mu k} ln \left(\frac{P^* - F}{P^* - (P_d + P_r)} \right). \tag{3}$$

The term $P_d + P_r$ is the load on the cross-section of the fiber at $z = l_d$ where l_d is the debond length. The quantity, P^*, is the axial force in the fiber that would be necessary to open the debonded portion of the interface if the fiber were being pulled from the composite, and P_r is the thermal residual axial force in the fiber. The expressions for P_r and P^* depend on $\sigma_N$and are also given in Kerans *et al.*

The extra displacement due to debonding is related to the applied load by assuming that the amount that the debonded portion of the fiber is compressed can be calculated with the following relation:

$$d = \frac{1 - 2\nu_f k}{\pi r_f^2 E_f} \int_0^{l_d} (P(z) - P_r) dz, \tag{4}$$

as

$$d = \frac{1 - 2\nu_f k}{2\mu k \pi r_f E_f} \left[F - P_d - P_r + (P^* - P_r) ln \left(\frac{P^* - F}{P^* - P_d - P_r} \right) \right]. \tag{5}$$

Equation (4) is based on the simple strength of materials expression for deflection, $\delta = FL/EA$, where the stiffness of the fiber is greater than E_f because it is not allowed to expand freely in the radial direction.

Finally, the following expression for mode II interfacial fracture toughness, G_{IIc}:

$$G_{IIc} = \frac{(1 - 2\nu_f k) P_d^2}{4\pi^2 r_f^3 E_f} \tag{6}$$

is based on the change in the compliance of the force–displacement data with respect to debond length. Equation (6) is based on the assumption that the interface debonds when the axial load in the fiber reaches a critical value. When eqn (6) is substituted into eqns (3) and (5), the following equations for force as a function of debond length and displacement as a function of debond length during progressive debonding are derived:

$$F = (C_1 G_{IIc}^{1/2} + P_r - P^*) e^{C_3 \mu l_d} + P^*, \tag{7}$$

$$d = \frac{C_2}{\mu}\left[F - C_1 G_{IIc}^{1/2} - P_r + (P^* - P_r) ln\left(\frac{P^* - F}{P^* - P_d - P_r}\right)\right]. \tag{8}$$

where C_1, C_2, and C_3 are constants that depend on material properties and r_f.

In the frictional problem the entire interface is debonded and the embedded length, (t+d) (d is negative by convention), determines the load required to slide the fiber with respect to the matrix. If the axial load is set to zero (instead of $P_d + P_r$) at $z = l_d$ and l_d is set to $t+d$ where t is the sample length, the following relation between force and displacement during frictional pushout results:

$$t + d = \frac{1}{C_3 \mu} ln \frac{P^* - F}{P^*} \tag{9}$$

Equations (7)–(9) are used in Section 6.3 to compare predicted debond length with the experimentally measured debond length.

6.2 *Determination of residual stresses*

The radial compressive stress at the fiber-matrix interface away from the fiber ends due to processing and/or roughness was found photoelastically before and after debonding to determine whether the additional radial compressive stress produced by fiber asperities after interface debonding was a significant factor. Samples twice as thick as the sample to which the curve in Fig. 8 corresponds were used so the surface effects region would be a less significant portion of the total thickness of the sample. The photoelastic measurement of the interface radial stress consisted of placing the pushout sample in the polariscope such that the fiber was parallel to the laser beam. The bright field and dark field isochromatic fringe patterns in the matrix were recorded and used to multiply the fringe order digitally by two times according to the method described by Toh *et al.* (1990). Due to the axisymmetry of the sample, the isoclinic fringe patterns were not required to separate the stresses. The radial stress at the interface away from the fiber ends was calculated from the resulting isochromatic fringe pattern using the shear difference method (Frocht, 1946). The pre- and post-debonding measurements of σ_N were both -5.68 MPa from which P_r and P^* were then calculated. A more detailed description of the measurement of σ_N is given in the Appendix.

6.3 *Comparison of measured and shear lag theory debond lengths*

The maximum load and corresponding displacement in section III of Fig. 8, P_r and P^* were substituted into eqn (9), and eqn (9) was solved for μ. The result was a coefficient of friction of 0.52. Published values for the coefficient of friction of a polyester/epoxy interface were not available in the literature, but the coefficients of friction for several common polymers including polymethyl methacrylate, polyethylene, and polystyrene sliding against an epoxy were tabulated by Yamaguchi (1990). The μ's range from 0.3–0.8. A μ of 0.52, determined with the current pushout test, falls within this range.

Once μ was known, force–displacement data derived from section II of Fig. 8 was fit to eqn (8) and an interfacial fracture toughness of 389 J/m^2 was obtained. The appropriate displacement to be used with Eq. (8) is the difference between the solid and dashed lines in section II of Fig. 8 since the displacement in the LH&KP solution is due to debond growth only. The curve fit for G_{IIc} is shown in Fig. 10. Although

G_{IIc} was iteratively least squares fit to the force–displacement data, the natural log term in eqn (8) remained small with respect to the other three terms on the right hand side. The small natural log term caused the curve fit to be approximately linear with the slope equal to C_2/μ. Hence, G_{IIc} was determined by only the intercept of the line fit through the force–displacement curve with the force axis. Since the slope of the line fit to the pushout data is reasonably close to the slope of the measured force–displacement curve, the coefficient of friction calculated from the initial frictional data point is consistent. Finally, the shear lag prediction of debond length was calculated by substituting μ and G_{IIc} into eqn (7).

A comparison of predicted debond length and experimentally measured debond length is shown in Fig. 11. The measured debond length is a nearly constant 1.5 fiber radii greater than the debond length predicted by shear lag theory. After debond initiation, the debond apparently grows easily through the surface effects region. Additional interface crack growth from that point on follows the prediction of shear lag since the slopes of the measured and predicted debond length curves are very close. Coincidentally, the interface crack growth becomes unstable at approximately 1.5 fiber radii from the bottom of the sample, so 1.5 fiber radii could be used as an estimate of the thickness of the surface effects region for this system. If a method were available to measure or estimate the size of the surface effects region for any composite, the shear lag solution could be modified to give a more accurate prediction of debond length, and therefore a more accurate prediction of interface toughness. For a given load, if the debond length is smaller, a smaller portion of the load is transferred to the matrix through friction in the debonded section of the sample, and the resulting axial load in the fiber near the debond tip is greater. A larger interface toughness will be needed to resist debond growth. Since the debond length for the current system is under-predicted, the interface toughness will be over-predicted.

If, instead of fitting the force–displacement data to eqn (8) and checking the predicted debond length, the measured debond length is fit to eqn (7) and the displacement is checked, the displacement is over-predicted. For the pushout curve shown in Fig. 8, this inverse procedure for fitting the experimental data to the shear lag model results in a $G_{IIc} = 105$ J/m^2. Consequently, the toughness calculated from the shear lag theory varies by a factor of three depending on how the pushout data is fit.

The larger value of interfacial toughness (389 J/m^2) calculated using shear lag theory appears to be extremely large. Strength values in terms of resistance to cracking for a polyester/epoxy interface are not available in the literature. Mode II measurements of epoxy interfaces with materials other than polyester have been conducted but were arrived at using the fiber pushout or pullout test and a shear lag analysis. The mode I critical strain energy release rate for an epoxy (crack within the material not at an interface) ranges from 50–200 J/m^2 (Young and Lovell, 1991). The mode I toughness of the matrix cannot be directly compared to the measured mode II toughness of the interface, but the value of the matrix toughness indicates that the smaller value of interfacial toughness (105 J/m^2) is probably more accurate. The larger value of G_{IIc} was determined by fitting the force–displacement data to eqn (8) while the smaller value was determined from eqn (7). Equation (8) requires an assumed expression for the deflection of the debonded portion of the fiber [eqn (4)] while eqn (7) does not. This assumption may be one of the key factors which caused the under-predicted debond length and over-predicted G_{IIc}.

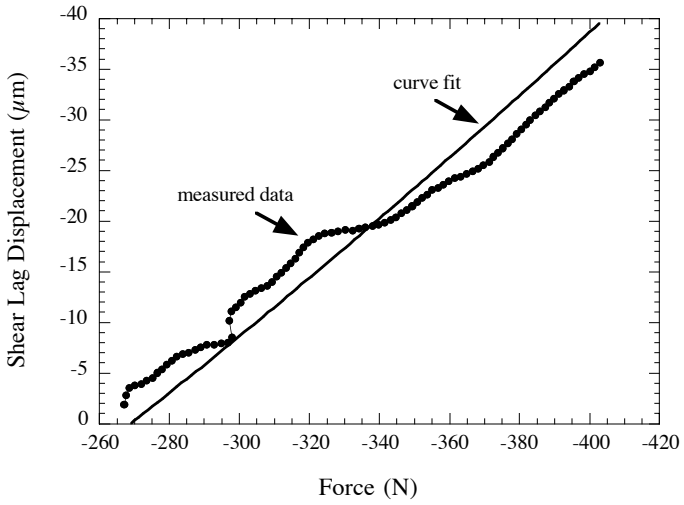

Fig. 10. Curve fit [eqn (8)] of measured force–displacement data for polyester/epoxy.

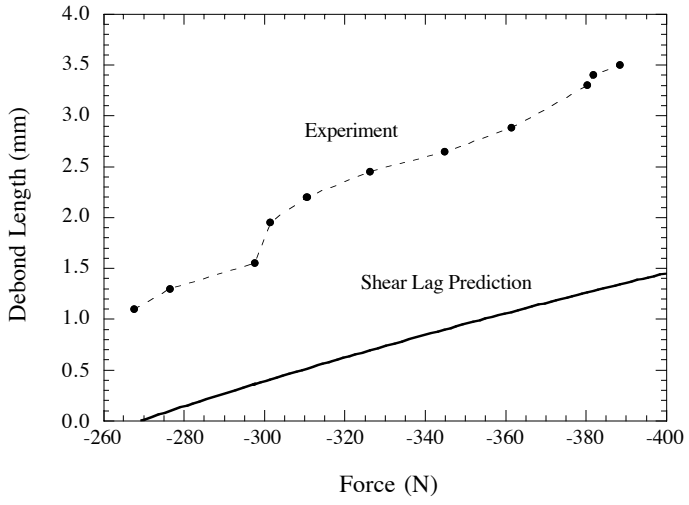

Fig. 11. Comparison of shear lag prediction and experimental measurement of debond length. P^* = 80.38 N, P_r = -45.83 N, μ = 0.52 , and G_{IIc} = 389 J/m^2.

7. ADDITIONAL EXPERIMENTAL OBSERVATIONS

The model composite experiments were also used to correlate interfacial failure processes with points on the fiber pushout load–displacement curve. During the initial linear part of the curve, there is no interfacial debond growth even if there is a debond present from processing. If the sample is thick enough, a debond initiates before the peak load is reached. At debond initiation there may be a small sharp load drop, but often, especially for a bottom debond, smooth transition to a shallower slope is observed before the load increases and the debond continues to grow. A similar nonlinearity in the force–displacement curve can also be caused by yielding of the fiber if it is necessary to apply an axial stress to the fiber that is larger than the local yield stress of the fiber. The length of the sample and the interface strength were chosen to be small enough in these tests so that no fiber damage occurred. The fiber top surface should always be inspected after a pushout test to determine whether damage has occurred. Once the debond was present, it grew toward the opposing surface until the debond growth became unstable within 1–4 fiber diameters of the surface, depending on the fiber-matrix–coating combination tested.

In systems such as glass and steel fibers in a room temperature cure epoxy the failure process was observed for very low residual stresses. The debond length was found at times to be significantly longer on one side of the fiber than on the other side. Also, for low residual stress composites, the debond tip often intermittently stopped and jumped forward rather than growing smoothly with increasing load as in the systems with larger residual stresses. This observation supports the findings of Eldridge (1995) who found that high residual stresses promoted stable debonding during the pushout test. Therefore, force–displacement data from a system with large residual stresses will most likely have less scatter.

Progressive debonding was observed in the model composites tested for thicknesses as small as 2.5 fiber diameters regardless of interface strength. Therefore, even qualitative comparisons of the average interfacial shear strengths ($F_{max}/\pi r_f^2$) from the pushout testing of the model composites would not provide useful information. Based on this observation, the calculations and comparisons of average interfacial shear strengths from the maximum applied load during pushout testing which are often found in the literature are questionable.

8. DISCUSSION AND CONCLUSIONS

Observations of the development of photoelastic fringe patterns in the matrix of several model composites during fiber pushout tests demonstrated that the linear part of the pushout curves corresponded to a fully bonded interface, the nonlinear part of the pushout curves up to the maximum load corresponded to progressive debonding, and the portion after the maximum load corresponded to frictional sliding of the totally debonded fiber. This correlation between the interface failure sequence and the pushout test force–displacement curve cannot necessarily be extended to all composites based on the model composite pushout tests, but it is evidence that the common interpretation of the profile of fiber pushout and pullout force–displacement curves is correct in many instances.

Testing of several model composites and correlation with results in the literature indicated that composite systems with a fiber–matrix modulus ratio of greater than 4

tend to debond from the bottom first during the pushout test. Therefore, the current shear lag models do not apply to these systems unless it has been determined through some independent test that the system in question debonds from the top. The only model composites tested that debonded from the top had an E_f/E_m ratio less than 3. Many composites of current interest will not debond from the top during pushout testing since both low and low residual stresses are necessary.

The debond length was measured as a function of applied load for a polyester/epoxy system that debonded from the top. The measured debond length was a nearly constant 1.5 fiber radii greater than the debond length predicted by the LH&KP shear lag solution. The under-predicted debond length is evidence that the shear lag model will over-predict the interface toughness when used to analyze pushout data. Although the assumptions of shear lag theory—infinitely long samples, infinite matrix radius, and debonds that have grown far from the top surface—were violated in the experiment, the lengths of the samples (2.5–3.0 fiber diameters long) that were tested for the debond length comparisons are not extremely small. Sample lengths of less than 5 fiber diameters are used in pushout testing of many metal, intermetallic, and ceramic matrix composites to avoid fiber damage or failure of the punch.

Finally, debond length versus displacement curves are shown for pushout tests on a composite that debonds from the bottom. The debond length measurements can be used to check the accuracy of theoretical solutions to the pushout problem if more advanced solutions are developed that include surface effects and/or the possibility of a bottom debond.

ACKNOWLEDGEMENTS

The authors would like to acknowledge the support of the ONR (under contract monitor R. Barsoum) and the AFOSR (Senior Knight Program). Also, we would like to thank Dr. N. J. Pagano from Wright Laboratory and Professor T. J. Mackin from the University of Illinois for the time, effort, and ideas they contributed to this project.

REFERENCES

Atkinson, C., Avila, J., Betz, E. and Smelser, R. E. (1982) The rod pull out problem, theory and experiment. *J. Mech. Phys. Solids* **30**, pp. 97–120.

Bao, G. and Song, Y. (1993) Crack bridging models for fiber composites with slip-dependent interfaces. *J. Mech. Phys. of Solids* **41**, pp. 1425–1444.

Brun, M. K. and Singh, R. N. (1988) Effect of thermal expansion mismatch and fiber coating on the fiber/matrix interfacial shear stress in ceramic matrix composites. *Adv. Cer. Mat.* **3**, pp. 506–509.

Cordes, R. D. and Daniel, I. M. (1995) Determination of interfacial properties from observations of progressive fiber debonding and pullout. *Comp. Eng.* **5**, pp. 633–648.

Daniel, I. M., Anastassopoulos, G. and Lee, J.-W. (1993) The behavior of ceramic matrix fiber composites under longitudinal loading. *Comp. Sci. Tech.* **46**, pp. 105–113.

Eldridge, J. I. (1995) Elevated temperature fiber push-out testing. *Mat. Res. Soc. Symp. Proc.* **365**, pp. 283–290.

Frocht, M. M. (1946) *Photoelasticity* **1**, pp. 252-285. Wiley, New York, Gao, Y.-C., Mai, Y.-W. and Cotterell, B.(1988) Fracture of fiber reinforced materials. *J. Appl. Math. Phys.* **39**, pp. 550–572.

Hsueh, C. H. (1990) Interfacial debonding and fiber pull-out stress of fiber-reinforced composites. *Mater. Sci. Eng.* **A123**, pp. 1–11.

Jero, P. D. and Kerans, R. J. (1990) The contribution of interfacial roughness to sliding friction of ceramic fibers in a glass matrix. *Scripta Metall. Mat.* **24**, pp. 2315–2318.

Kerans, R. J. and Parthasarathy, T. A. (1991) Theoretical analysis of the fiber pullout and pushout tests. *J. Am. Ceram. Soc.* **74**, pp. 1585–1596.

Kline, G. E. (1995) Photoelastic determination of in-plane stresses in shape memory alloy/polymer matrix composites. M.S. thesis, Department of Theoretical and Applied Mechanics, University of Illinois at Urbana-Champaign.

Koss, D. A., Hellman, J. R. and Kallas, M. N. (1993) Fiber pushout and interfacial shear in metal-matrix composites, *JOM* **45** March, pp. 34–37.

Laughner, J. W., Shaw, N. J., Bhatt, R. T. and Dicarlo, J. A. (1986) Simple indentation method for measurement of interfacial shear strength in SiC/Si3N4 composites. *Cer. Eng. and Sci. Proc.* **7**, pp. 932.

Liang, C. and Hutchinson, J. W. (1993) Mechanics of the fiber pushout test. *Mech. of Mat.* **14**, pp. 207–221.

Mackin, T. J., Yang, J. and Warren, P. D. (1992) Influence of fiber roughness on the sliding behavior of sapphire fibers in TiAl and glass matrices. *J. Am. Ceram. Soc.* **75**, pp. 3358–3362.

Marshall, D. B. and Oliver, W. C. (1990) An indentation method for measuring residual stresses in fiber-reinforced ceramics. *Mater. Sci. Eng.* **A126**, pp. 95-103.

Netravali, A. N., Stone, D., Ruoff, S. and Topoleski, L. T. (1989) Continuous microindenter push-through technique for measuring interfacial shear strength of fiber composites. *Comp. Sci. Tech.* **34**, pp. 239–303.

Toh, S. L., Tang, S. H. and Hovanesian, J. D. (1990) Computerized photoelastic fringe multiplication. *Exp. Tech.* **14** July/Aug., pp. 21–23.

Tsai, K.-H. and Kim, K.-S. (1991) A study of stick slip behavior in interface friction using optical fiber pull out experiment. *SPIE, Speckle Techniques, Birefringence Methods, and Applications to Solid Mechanics* **1554A**, pp. 529–541. Tsai, K.-H. and Kim, K.-S. (1996) The micromechanics of fiber pull-out. *J. Mech. Phys. Solids* **44**, pp. 1147–1177.

Warren, P. D., Mackin, T. J. and Evans, A. G. (1992) Design, analysis, and application of an improved push-through test for the measurement of interface properties in composites. *Acta Metall. Mater.* **40**, pp. 1243–1249.

Watson, M. C. and Clyne, T. W. (1992) The use of single fibre pushout testing to explore interfacial mechanics in SiC monofilament-reinforced TiI. A photoelastic study of the test. *Acta. Metall. Mater.* **40**, pp. 131–139.

Yamaguchi, Y. (1990) *Tribology of Plastic Materials*, pp. 52–88. Elsevier, New York.

Young, R. J. and Lovell, P. A. (1991) *Introduction to Polymers*, pp. 394–407. Chapman and Hall, New York.

APPENDIX: MATRIX SHRINKAGE MEASUREMENT

The EPON 828 resin and DETA curing agent mixture was cured at room temperature. Both chemical shrinkage of the matrix and volume changes due to heat generated by the chemical reaction occurred during cure. The chemical shrinkage of the fiber during cure could not be found in the literature; therefore, the average radial stress at the interface for the polyester/epoxy (DETA) system was measured photoelastically and used to calculate indirectly the differential shrinkage between the polyester fiber and epoxy matrix. The fiber and matrix elastic properties and the dimensions of the photoelastic sample were used in a finite element simulation of processing. A differential shrinkage strain of 0.0022 was calculated in the finite element simulation by isotropically shrinking the matrix around the fiber until an average interfacial radial stress of -5.68 MPa was produced. The derivation of the relation between the photoelastic fringe order and the average interfacial radial stress at the interface is presented below.

The coordinate system, the relevant dimensions, and a schematic of the circular photoelastic fringes that were observed in the epoxy matrix are shown in Fig. A1. The derivation draws on one of the two dimensional equilibrium equations in Cartesian coordinates:

$$\frac{\partial \sigma_{xx}}{\partial x} + \frac{\partial \sigma_{xy}}{\partial y} = 0. \tag{A.1}$$

The Fundamental Theorem of Calculus was used to write an expression relating the known value of σ_{xx} at one position (x_0, y_0) to the unknown value of σ_{xx} at another position (x, y_0):

$$\int_{x_o}^{x} \frac{\partial \sigma_{xx}(x, y_0)}{\partial x} dx = \sigma_{xx}(x, y_0) - \sigma_{xx}(x_0, y_0). \tag{A.2}$$

Substitution of eqn (A2) into eqn (A1) yields one of the shear difference equations from Frocht (1946):

$$\sigma_{xx}(x, y_0) = \sigma_{xx}(x_0, y_0) - \int_{x_o}^{x} \frac{\partial \sigma_{xy}(x, y_0)}{\partial y} dx. \tag{A.3}$$

Also, from Frocht (1946), the photoelastic fringe order is related to the principal stresses according to the relation

$$\sigma_1 - \sigma_2 = \frac{N f_\sigma}{h}, \tag{A.4}$$

where N is the fringe order, h is the sample thickness (7.8 mm), f_σ is the material fringe constant [10.49 N/mm for EPON 828/DETA, (Kline, 1995)], and and σ_1 and σ_2 are the maximum and minimum principal stresses. The principal stresses are related to the σ_{xy} shear stress by the Mohr's Circle relation

$$\sigma_{xy} = \frac{\sigma_1 - \sigma_2}{2} sin(2\theta), \tag{A.5}$$

where θ is the angle between the x axis and the direction of the minimum principal stress. Equations (A4) and (A5) are combined and θ is written in terms of the x and y coordinates:

$$\sigma_{xy}(x,y) = \frac{N(x,y) f_\sigma}{2h} sin\left[2tan^{-1}\left(\frac{y}{x}\right)\right]. \tag{A.6}$$

The partial derivative of $\sigma_{xy}(x,y)$ is computed with respect to y and evaluated at $y = 0$:

$$\frac{\partial \sigma_{xy}(x,0)}{\partial y} = \frac{f_\sigma}{h} \frac{N(x,0)}{x} \tag{A.7}$$

Along the x axis, the radial stress is the same as σ_{xx}, and both are zero on the x axis at $x = r_0$. This information and the substitution of eqn (A7) into eqn (A3) yields an expression for the radial stress (averaged through the sample thickness) at the interface:

$$\sigma_{rr}(x = r_f, y = 0) = \frac{-f_\sigma}{h} \int_{r_0}^{r_f} \frac{N(x, y = 0)}{x} dx. \tag{A.8}$$

The fringe order as a function of the radial coordinate must be measured to calculate the radial stress at the interface.

A light field image of the photoelastic fringes near the fiber surface in the matrix of a steel/epoxy sample is shown in Fig. A2. A steel/epoxy image is shown rather than a polyester/epoxy image because in the latter the fringes are sparse and the image must be magnified near the fiber to distinguish the fringes from the fiber. The steel/epoxy photoelastic fringe pattern in Fig. A2 illustrates the concept more clearly.

Light and dark field images were recorded of the photoelastic fringe pattern in a 7.8 mm long polyester/epoxy sample. The pixel intensities of the dark field image were subtracted from the pixel intensities of the light field image to produce an image with twice the fringes to increase the resolution. No significant difference in fringe order as a function of radius could be determined between images taken before and after total debond. The fringe order could not be measured exactly at the fiber surface since the closest fringe to the fiber was a finite distance from the fiber surface. Quadratic splines were fit through the fringe order versus radius data points to obtain a continuous function of fringe order versus radius that was then extrapolated to the fiber surface. This function was used in eqn (A8) and an average radial stress at the interface of -5.68 MPa was calculated. The variation of radial stress from the outer edge of the sample to the fiber surface is shown in Fig. A3.

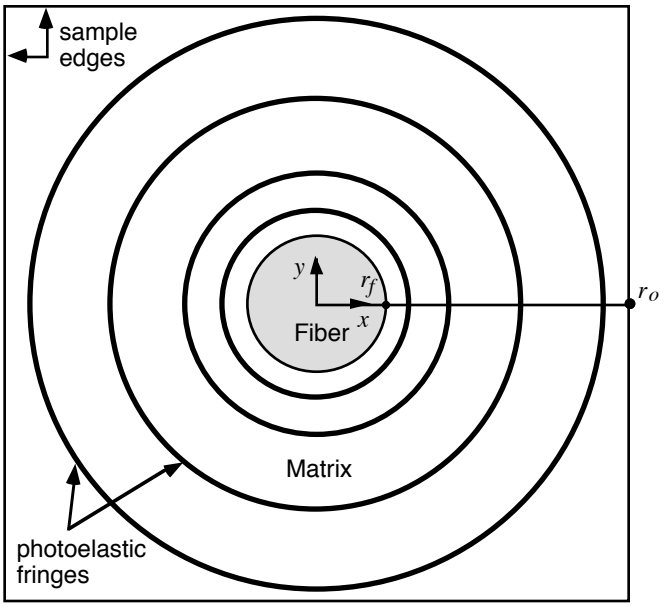

Fig. A1. Geometry for the derivation of the relation between fringe order and average interfacial radial stress.

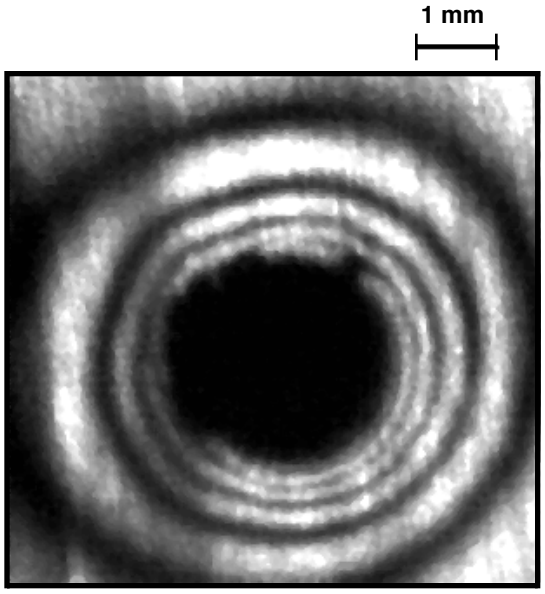

Fig. A2. Photoelastic fringe patterns surrounding the fiber in a steel/epoxy pushout sample.

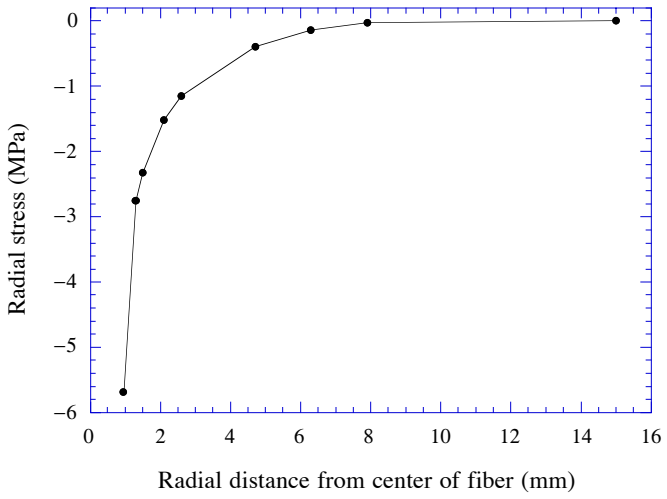

Fig. A3. Thickness average of radial stress in matrix as a function of distance from the fiber center in a 7.8 mm thick polyester/epoxy fiber pushout sample as calculated from the photoelastic fringe pattern.